ELSEVIER

Journal of Contaminant Hydrology 57 (2002) 259–279

JOURNAL OF Contaminant Hydrology

www.elsevier.com/locate/jconhyd

Two-site kinetic modeling of bacteriophages transport through columns of saturated dune sand

Jack F. Schijven [a,1], S. Majid Hassanizadeh [b,*], Ria H.A.M. de Bruin [a,2]

[a] *National Institute of Public Health and the Environment, Microbiological Laboratory for Health Protection, P.O. Box 1, 3720 BA Bilthoven, The Netherlands*

[b] *Delft University of Technology, Faculty of Civil Engineering and Geosciences, P.O. Box 5048, 2600 GA Delft, The Netherlands*

Received 13 August 2001; received in revised form 30 November 2001; accepted 3 December 2001

Abstract

Breakthrough curves, on a semi-log scale, from tests in porous media with block-input of viruses, bacteria, protozoa and colloidal particles often exhibit a typical skewness: a rather slowly rising limb and a smooth transition of a declining limb to a very long tail. One-site kinetic models fail to fit the rising and declining limbs together with the tail satisfactorily. Inclusion of an equilibrium adsorption site does not seem to improve simulation results. This was encountered in the simulation of breakthrough curves from a recent field study on the removal of bacteriophages MS2 and PRD1 by passage through dune sand. In the present study, results of laboratory experiments for the study of this issue are presented. Breakthrough curves of salt and bacteriophages MS2, PRD1, and ϕX174 in 1D column experiments have been measured. One- and two-site kinetic models have been applied to fit and predict breakthrough curves from column experiments. The two-site model fitted all breakthrough curves very satisfactorily, accounting for the skewness of the rising limb as well as for the smooth transition of the declining limb to the tail of the breakthrough curve. The one-site model does not follow the curvature of the breakthrough tail, leading to an overestimation of the inactivation rate coefficient for attached viruses. Interaction with kinetic site 1 is characterized by relatively fast attachment and slow detachment, whereas attachment to and detachment from kinetic site 2 is fast. Inactivation of viruses and interaction with kinetic site 2 provide only a minor contribution to removal. Virus removal is mainly determined by the attachment to site 1. Bacteriophage ϕX174 attached more than MS2 and PRD1, which can be explained by the greater

* Corresponding author. Tel.: +31-15-278-7346.

E-mail addresses: Jack.Schijven@rivm.nl (J.F. Schijven), Majid.Hassanizadeh@ct.tudelft.nl (S.M. Hassanizadeh), Ria.de.Bruin@rivm.nl (H.A.M. de Bruin).

[1] Tel.: +31-30-274-2994.

[2] Tel.: +31-30-274-3929.

PII: S0169-7722(01)00215-7

electrostatic repulsion that MS2 and PRD1 experience compared to the less negatively charged ϕX174.

Keywords: Bacteriophages; Virus transport; Column experiments; MS2; PRD1; ϕX174; Kinetic modeling

1. Introduction

Removal of microorganisms from water due to passage through soil is of great importance in drinking water production. In the Netherlands, about 14% of the total drinking water is produced from pre-treated surface water that is artificially recharged in dune areas. No chlorination of water is applied and the adequate removal of microorganisms is for the most part dependent on the efficiency of removal by passage through soil. Also, delineation of wellhead protection zones against microbial pollution is based on the removal capacity of soils. There have been numerous studies to identify various removal processes and quantify their share in overall removal of microorganisms. Commonly, these studies involve the measurement of breakthrough curves in the field or laboratory column experiments (see Schijven and Hassanizadeh, 2000 for an extensive review). It is well known that kinetic adsorption is a very important process in virus removal. Usually, an advection–dispersion model, including one-site kinetic attachment as well as first-order inactivation, is employed to simulate measured breakthrough curves.

Often, semi-log plots of breakthrough curves from tests with block-input of viruses (Bales et al., 1991, 1993; DeBorde et al., 1999; Dowd et al., 1998; Fujito and Lytle, 1996), bacteria (Hornberger et al., 1992; Johnson et al., 1995; Lindqvist et al., 1994; Kinoshita et al., 1993; McCaulou et al., 1994; Tan et al., 1994), *Cryptosporidium* (Harter et al., 2000) and colloidal particles (van de Weerd et al., 1998) exhibit a typical skewness: a rather slowly rising limb and a smooth transition of a declining limb to a very long tail. It is known that one-site kinetic models fail to fit the rising and declining limbs together with the tail satisfactorily (Bales et al., 1991; Harter et al., 2000; Hornberger et al., 1992; Lindqvist et al., 1994; McCaulou et al., 1994; Tan et al., 1994). There are models where one kinetic reversible adsorption site and one equilibrium site are assumed to be present (cf. Bales et al., 1991; Toride et al., 1995). It is often shown that the contribution of equilibrium adsorption to virus attenuation is negligible (see, e.g., Bales et al., 1991, 1997; Schijven and Hassanizadeh, 2000). There are yet other models where one reversible kinetic site and one irreversible adsorption site are assumed. For example, in one study on bacterial transport (Johnson et al., 1995), it was shown that a model that assumed a time-dependent detachment function and a limited number of favorable irreversible attachment sites, could simulate the rising and climbing limbs of the breakthrough curve satisfactorily. In that study, however, the tails were measured for a short period only. Recently, in a study on the removal of viruses in unsaturated porous media (Chu and Jin, 2001), two kinetic adsorption sites were considered: adsorption to soil surfaces as well as adsorption to the air–water interface. But, the possibility of presence of two kinetic reversible adsorption sites in saturated soil has so far not been investigated.

In the present study, we investigate the possibility that more than one type of kinetic site may be present. Kinetic sites with different rates of attachment and detachment may exist

due to surface charge heterogeneity of the granular medium and/or physical non-equilibrium. Patch-wise charge heterogeneities are common to all aqueous geologic settings, originating from inherent differences in the surface properties of adjacent crystal faces on mineral grains, and from minerals having bulk- or surface-bound chemical impurities (Ryan and Elimelech, 1996). Physical non-equilibrium results from the exchange of particles or solutes between mobile and immobile regions (Toride et al., 1995).

Recently, a series of field and laboratory experiments have been carried out in order to gain insight in virus removal processes in dune sand and developing conceptual models for quantitative modelling of these processes (Schijven, 2001). An extensive field study was carried out in the dune area of Castricum, The Netherlands. This was aimed at investigating the effectiveness of dune recharge for virus removal (Schijven et al., 1999). Recharge water was dosed with bacteriophages MS2 and PRD1 for 11 days at a constant concentration in a 10×15 m compartment that was isolated in a recharge basin. Breakthrough was monitored for 120 days at six wells with their screens located along a calculated flow line. Concentrations of both phages were reduced about 3 $\log_{10}$ over the first 2.4 m and 5 $\log_{10}$ over the next 27 m. To clarify this nonlinear removal, column experiments were carried out under similar conditions as in the field: same recharge water, temperature (5 ± 3 °C) and pore water velocity (1.5 m day^{-1}) (Schijven, 2001). Soil samples were taken along a streamline between the recharge canal and the first monitoring well. Bacteriophage ϕX174 was included for comparison. The high initial removal in the field was found not to be due to heterogeneity of phage suspensions but to soil heterogeneity. Phage removal rates correlated strongly positively with soil organic carbon content, and relatively strongly positively with silt content and the presence of ferric oxyhydroxides (Schijven, 2001). Note that here we are not referring to microscale grain surface charge heterogeneities but to macroscale spatial heterogeneities.

The experiments reported here were designed to closely simulate field conditions. To that aim, two different columns were filled with saturated sand from the field. Water from the recharge canal was used. The experiments were all conducted in a cold room at the same temperature as that of the groundwater during the field study. The same transport velocity as in the field (1.5 m day^{-1}) was applied. Presence of physical non-equilibrium was investigated with the aid of salt breakthrough curves. Also, breakthrough curves of bacteriophages MS2, PRD1 and ϕX174 were measured. The latter phage was included because it is less negatively charged than MS2 and PRD1, and may therefore interact differently with kinetic sites for attachment. A two-site kinetic model was constructed and its ability to simulate the breakthrough curves better in comparison to a one-site kinetic model was studied. The laboratory experiments reported here serve to increase our insight in the role kinetic adsorption in the modelling of virus removal.

2. Experimental methods

2.1. Microorganisms

Highly concentrated suspensions of MS2 and PRD1 were prepared as described in the Castricum field study (Schijven et al., 1999). A highly concentrated suspension of ϕX174

was prepared as described in ISO 10705-2 (2000b). A portion of each suspension was diluted with 1 g l^{-1} peptone–saline to a concentration of 10^{10}–10^{11} phages l^{-1}. These were used as stock suspensions. Prior to each experiment, aliquots from the stock suspensions of all three bacteriophages were diluted 1000-fold in a container with canal water for seeding. MS2 and PRD1 were selected as model viruses because of their negative charge. MS2 is an icosahedral phage with a diameter of 27 nm and a low isoelectric point (pI) of 3.5. PRD1 is an icosahedral bacteriophage with a diameter of 62 nm with an inner lipid membrane (Bales et al., 1991; Caldentey et al., 1990). Its pI lies between 3 and 4 (Loveland et al., 1996). Bacteriophage ϕX174 has a pI of about 6.6 and a size of 23 nm (Fujito and Lytle, 1996; Jin et al., 1997).

MS2 and PRD1 are the most hydrophobic viruses, but ϕX174 exhibits little, if any, hydrophobic character (Lytle and Routson, 1995; Shields and Farrah, 1987).

2.2. Packing of columns

A sample of about 50 kg of dune sand from the Castricum field site was taken near the screen of the first monitoring well at a distance of 2.4 m. The sample was kept saturated with canal water and transported in stainless steel buckets. Samples of canal water were also collected in 20-l polyvinylchoride containers. The sand and water samples were stored at 5 ± 3 °C. Only the sand and water from the field site were used for packing laboratory columns and performing virus transport experiments.

Fig. 1 shows a schematic representation of a column; a Perspex pipe with an inner diameter of 9 cm and a length of 1.9 m. A stainless steel grid for supporting the sand was placed at the bottom of the pipe. A stainless steel table supported the column. Along the pipe, 14 small stainless steel samplers were placed at 10-cm intervals. The pipe was filled with saturated dune sand at small increments. During the filling, canal water was flowing upwards. At the same time, the pipe was being tapped in order to distribute the sand evenly and to dislodge any air bubbles. The pipe was filled up to a length of 1.5 m. Initially, a thin layer of very fine sand particles settled on top of the column. This layer was removed by suction in order to create the same conditions as in Castricum field experiments. Note that no fine particles were removed during the filling of column. Thus, any fine particles originally present within the sand stayed behind. After 1–2 days, the flow of water was reversed to downward direction at a rate of 2.4 ml min^{-1}; resulting in a pore water velocity of about 1.5 m day^{-1}, the same as in the field. The sand column was kept saturated at all times. The water in the funnel-shaped outlet of the column was gently, but continuously, mixed by means of a magnetic stirrer. This way, the concentration gradient at the lower boundary of the column was kept to zero. In all experiments, pH of the recharge water was 7.5–8.0. At the inlet, canal water containing salt or microorganisms were pumped into the inflow reservoir. The overflow kept the

Fig. 1. Schematic representation of a column, filled with sand to a length of 1.5 m. Inner column diameter is 9 cm. At the inlet canal water was pumped and salt and microorganisms were seeded. The overflow kept the level of water above the column constant and led excess of water to the feeding tank. The pump that was connected to the outlet determined the flow rate of water through the column and led the effluent to a disposal tank. Numbers 1–14 represent stainless steel samplers, each 10 cm apart.

water at a constant head and returned excess water to the feed tank. The pump that was connected to the outlet regulated the flow rate of water through the column and sent the effluent to a disposal tank.

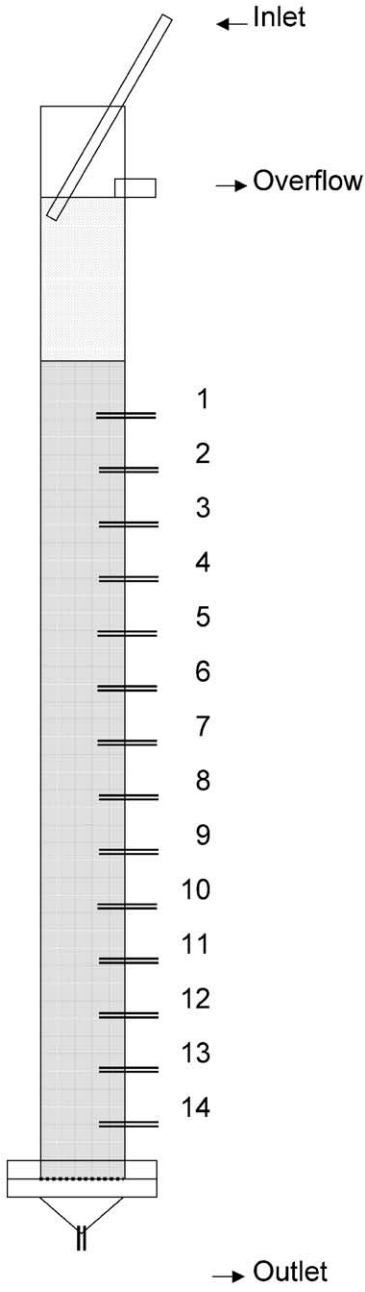

Two columns were prepared. Column I was operated at a pore water velocity of 1.5 m day^{-1} and column II at about twice this velocity.

2.3. Salt tracer experiments

For each column that was constructed, a salt transport experiment was carried out to serve two purposes: (i) to estimate interstitial flow velocity and medium dispersivity and (ii) to investigate the presence of kinetic effects due to the exchange of solutes between mobile and immobile regions. First, the water reservoir on top of the column was emptied by pumping to the point where less than 1 mm of water was left on top of the column. Then, it was filled gently with a solution of 750 mg l^{-1} sodium chloride in canal water up to the level of the overflow. This way, a sharp front of salt water was introduced into the sand column. The salt solution was fed for a period of 24 h. At the end of the dosage, the salt solution was replaced by canal water following the same procedure as at the start of the dosage. All samples were taken from sampler number 14 (at a depth of 1.4 m). Sampling was carried out by continuously pumping from the sampler at a rate of about 0.2 ml min^{-1} for 18 min per sample. Samples were collected in glass tubes using a programmable fraction collector. Concentration of the salt solution was determined by manually measuring electrical conductivity of the sampled fractions.

2.4. Transport experiments with bacteriophages

Suspensions of bacteriophages with concentrations of 10^7–10^8 phages l^{-1} were seeded for 24 h and breakthrough was monitored for a period of about a week. Seeding of the phages was carried out following the same procedure as explained for the salt tracer. Bacteriophages were sampled at sampler number 14 at the depth of 1.4 m at a rate of 0.2 ml min^{-1}. Samples were collected automatically every 6 min in glass tubes. Thus, over a period of 7 days, 1680 samples were collected. For each breakthrough curve of a bacteriophage, about 70–140 samples were analyzed. The sample collection tubing consisted of PTFE and silicone. Prior to each experiment, the tubing was rinsed with a chlorine solution and then with hot tap water. The tubing was tested for interaction with bacteriophages. This was done by pumping suspensions of bacteriophages through the tubing at a rate of 0.2 ml min^{-1}. Eight replicate influent and effluent samples were analyzed for bacteriophages. Analysis of variance showed no significant differences between influent and effluent concentrations. Therefore, we were sure that no attachment of bacteriophages to the tubing occurred.

2.5. Enumeration of bacteriophages

MS2 was assayed as described in ISO 10705-1 (2000a) using host strain WG49 (Havelaar et al., 1984). PRD1 was assayed according to ISO 10705-1 using *S. typhimurium* LT2 as the host, omitting nalidixic acid in the top agar layer. Bacteriophage ϕX174 was assayed according to ISO10705-2 (2000) using WG5 (ACTC 700078) as the host.

3. Modeling methods

3.1. Conceptual model

Major processes controlling the transport and removal of viruses in porous media are advection, dispersion, sorption (attachment and detachment), and inactivation of both free and adsorbed viruses. Both equilibrium and kinetic models have been used for modeling sorption of viruses. The role of equilibrium sorption is often found to be negligible (Schijven and Hassanizadeh, 2000). In fact, most researchers have described sorption of viruses by a linear kinetic model; that is, linear attachment and linear detachment occurring at different rates. Commonly, the attachment rate coefficient is much larger than the detachment rate coefficient. In the Castricum field study, we employed a one-site linear kinetic sorption model for the simulation of breakthrough curves. Although the breakthrough curve could be simulated reasonably well, there was a significant discrepancy at the end of the rising limb and at the start of the declining limbs of the breakthrough curves (Schijven et al., 1999). It was speculated that the presence of more than one type of kinetic site could be responsible for this shortcoming of the one-site kinetic model. To investigate whether multiple kinetic sites were present in the Castricum dune sands, a two-site kinetic model was constructed and used for analyzing bacteriophages breakthrough curves obtained in laboratory and field experiments. The aim has been to determine whether rate constants for the two kinetic sites are identifiable. The governing equations for an advection–dispersion model, including reversible adsorption to two types of kinetic sites and inactivation of free and attached bacteriophages, in the case of uniform one-dimensional flow, are as follows:

$$\frac{\partial C}{\partial t}+\frac{\rho_B}{n}\frac{\partial S_1}{\partial t}+\frac{\rho_B}{n}\frac{\partial S_2}{\partial t}=\alpha_L v\frac{\partial^2 C}{\partial x^2}-v\frac{\partial C}{\partial x}-\mu_l C-\mu_{s1}\frac{\rho_B}{n}S_1-\mu_{s2}\frac{\rho_B}{n}S_2 \quad (1)$$

$$\frac{\rho_B}{n}\frac{\partial S_1}{\partial t}=k_{att1}C-k_{det1}\frac{\rho_B}{n}S_1-\mu_{s1}\frac{\rho_B}{n}S_1 \quad (2)$$

$$\frac{\rho_B}{n}\frac{\partial S_2}{\partial t}=k_{att2}C-k_{det2}\frac{\rho_B}{n}S_2-\mu_{s2}\frac{\rho_B}{n}S_2 \quad (3)$$

where C is concentration of free phages [pfu/m^3]; S is concentration of attached phages [pfu/kg]; t is time [day^{-1}]; x is distance [m]; α_L is dispersivity [m]; v is average interstitial water velocity [m day^{-1}]; ρ_B is dry bulk density [kg/m^3]; n is porosity [−]; k_{att} and k_{det} are attachment and detachment rate coefficients, respectively [day^{-1}]; μ_l and μ_s are inactivation rate coefficients of free and attached phages, respectively [day^{-1}]. Subscripts 1 and 2 refer to the two different kinetic sites. These equations are subject to boundary conditions $C=C_0$ at $x=0$ and $\partial C/\partial x=0$ at $x=L$. The initial conditions were zero concentration for all phages.

A numerical model called EQ2KIN was constructed for solving the equations. The equations were discretized using an explicit central finite difference scheme.

Fitting of the breakthrough curves was carried out using log-transformed concentrations. The justification for this choice is as follows. Dilutions of the samples were made to obtain an approximately constant counting range in each plate. Within each analyzed dilution, phages are approximately Poisson-distributed. Poisson distribution implies that mean and variance are the same. Since mean counts were approximately constant, this also applies for the variance. To obtain concentrations, counts are multiplied by their corresponding dilution factor. Due to this multiplication, the errors in the observed concentrations will be approximately constant after log-transformation.

As a measure of goodness-of-fit, the coefficient of determination r^2 (Toride et al., 1995) was calculated on the basis of N logarithmically transformed observations C_i and fitted values F_i:

$$r^2 = 1 - \frac{\sum_{i=1}^{N} (\ln C_i - \ln F_i)^2}{\sum_{i=1}^{N} \left(\ln C_i - \frac{\sum_{i=1}^{N} \ln C_i}{N} \right)^2} \tag{4}$$

For comparison, a one-site kinetic model was also used for fitting of the breakthrough curves. To that aim, the same procedure was followed as for fitting of the two-site kinetic model, but the parameter values for site 2 were set to zero.

Under steady-state conditions, the relative contributions of inactivation and adsorption to the removal of viruses by soil passage can be computed analytically. A steady-state situation occurs when input of virus continues for a long time and may be seen as a worst-case situation. For a steady-state situation, Eqs. (1)–(3) are simplified to:

$$\alpha_L v \frac{\partial^2 C}{\partial x^2} - v \frac{\partial C}{\partial x} = \mu_1 C + \mu_{s1} \frac{\rho_B}{n} S_1 + \mu_{s2} \frac{\rho_B}{n} S_2 \tag{5}$$

$$\frac{\rho_B}{n} S_1 = \frac{k_{att1}}{\mu_{s1} + k_{det1}} C \tag{6}$$

$$\frac{\rho_B}{n} S_2 = \frac{k_{att2}}{\mu_{s2} + k_{det2}} C \tag{7}$$

Substitution of Eqs. (6) and (7) into Eq. (5) gives:

$$\alpha_L \frac{\partial^2 C}{\partial x^2} - \frac{\partial C}{\partial x} - \frac{\lambda}{v} C = 0 \tag{8}$$

where

$$\lambda = \mu_1 + \frac{k_{att1}}{1 + k_{det1}/\mu_{s1}} + \frac{k_{att2}}{1 + k_{det2}/\mu_{s2}} \tag{9}$$

Now, Eq. (8) has the following solution:

$$\log_{10}\left(\frac{C}{C_0}\right) = \frac{x}{2.3}\,\frac{\left(1 - \sqrt{1 + 4\alpha_L \frac{\lambda}{v}}\right)}{2\alpha_L} \tag{10}$$

where C_0 is concentration at $x = 0$, and $\log(C/C_0)$ is a measure of virus removal.

The term λ in Eq. (9) is equivalent to an overall removal rate coefficient. It is evident from Eq. (9) that three terms contribute to the overall removal rate. The first term is due to the inactivation of free viruses. The second and last terms give the removal rate of viruses due to interaction with the two kinetic sites. Interaction means the combination of attachment, detachment and inactivation of attached viruses. The parameter values obtained from fitting the breakthrough curves were employed to calculate the removal rates and the contribution of inactivation and interaction with both kinetic sites under steady-state conditions.

3.2. Calculation of collision efficiencies

In colloid filtration theory of attachment, the parameter "collision efficiency" is introduced as a measure of the intrinsic capacity of the soil for adsorption (Yao et al., 1971). The collision efficiency is an empirical constant that accounts for electrostatic interactions, in this case, between bacteriophages and the porous medium. Collision efficiency, α, is calculated using the following equation (Yao et al., 1971):

$$\alpha = \frac{2}{3}\,\frac{d_c}{(1-n)}\,\frac{k_{att}}{v}\,\frac{1}{\eta} \tag{11}$$

where α is collision efficiency, η is single collector efficiency and d_c is grain size [m]. Bacteriophages are small in size and their transport in the immediate vicinity of the soil grains is dominated by Brownian diffusion. Thus, the single collector efficiency η is determined from the following formula (Penrod et al., 1996):

$$\eta = 4A_s^{1/3} N_{Pe}^{-2/3} \tag{12}$$

where $N_{Pe} = d_p v n / D_{BM}$ accounts for diffusion, $D_{BM} = K_B(T + 273)/(3\pi d_p \mu)$ is diffusion coefficient [$m^2\ s^{-1}$] with Boltzmann constant $K_B = 1.38 \times 10^{-23}$ (J K^{-1}), d_p represents virus particle size [m] and T is water temperature [°C]. $A_s = 2(1-\gamma^5)/(2 - 3\gamma + 3\gamma^5 - 2\gamma^6)$ is Happel's porosity-dependent parameter, with $\gamma = (1-n)^{1/3}$. Eqs. (11) and (12) were employed to calculate collision efficiencies α_1 and α_2, from estimates of k_{att1} and k_{att2}, respectively.

4. Results

4.1. Analysis of salt breakthrough curves

Fig. 2 shows observed and fitted salt breakthrough curves from both columns I and II. As can be seen, salt behaves as a conservative tracer; a steady-state value of $C/C_0 = 1$ is reached and excellent fits of the breakthrough curves have been obtained. In addition to the two column experiments presented here, we did several other salt tracing experiments in other columns (data not shown). In all of these experiments, salt behaved as a conservative tracer. In the case of the salt BTC from column II, we see an apparent tailing. But that is most probably due to drifting of the EC meter as the EC drops below the background value. Therefore, we may conclude that there are no physical non-equilibrium effects present in these columns.

Salt breakthrough curves were used to estimate medium porosity and dispersivity. Corresponding values are listed in Table 1 where also values from Castricum field study are reported.

4.2. Analysis of phages breakthrough curves

Figs. 3, 5a–5e show the measured and simulated breakthrough curves in column I. Our model EQ2KIN was coupled to parameter estimation code PEST version 1.07 (Watermark Computing, 1994) in order to determine adsorption parameter values from column I breakthrough curves. Both one-site and two-site kinetic adsorption parameter values were estimated. These were k_{att1}, k_{att2}, k_{det1}, k_{det2} and μ_{s1}. The value of parameter μ_{s2} was assumed to be equal to μ_{s1}. The inactivation rate of phages in water, μ_l, were found in another series of experiments (Schijven, 2001) by measuring their inactivation in

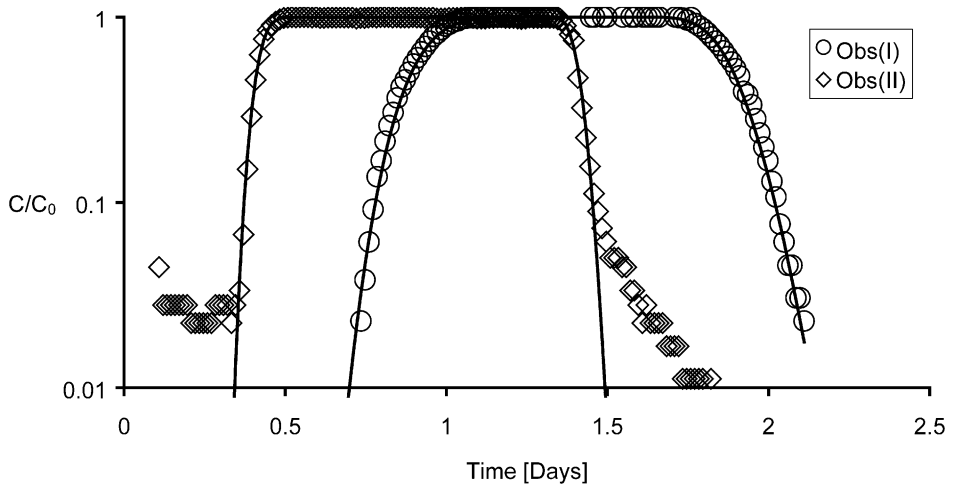

Fig. 2. Measured salt breakthrough curves Obs(I) and Obs(II) from column experiments I and II and fitted breakthrough curves (solid lines).

Table 1
Experimental conditions of column experiments and of first two monitoring wells in the Castricum field study, W1 and W2

Column or well no.	I	II	W1[a]	W2[a]
Travel distance [m]	1.41	1.42	2.4	3.8
v [m day^{-1}]	1.6	3.5	1.4	1.6
α_L [m]	0.0075	0.0043	0.0080	0.012

[a] Data from field study (Schijven et al., 1999). Porosity 0.35.

suspensions made from column influent and effluent samples for a period of 1–2 weeks. The estimated μ_l values were 0.082 day^{-1} (MS2), 0.044 day^{-1} (PRD1) and 0.012 day^{-1} (ϕX174).

Fig. 3 shows the measured breakthrough curve of MS2 in column I. First, a one-site kinetic model was applied to fit this curve with the concentrations on a linear scale using EQ2KIN and setting parameter values for site 2 to zero. Values for k_{att1}, k_{det1} and μ_{s1} are given in Table 2, under heading A, and correspond with curve A in Fig. 3. Curve A fits the measured breakthrough curve very well except for the tail part. This is not considered as satisfactory because the tails contain important information on the inactivation rate of attached phages (Schijven et al., 1999). Indeed, parameter values appear to be unrealistic. The value of k_{det1} is unexpectedly higher than that of k_{att1} and the value of μ_s determined here is 50 times higher than the value of μ_l. In an analysis of virus inactivation from batch experiments (Schijven and Hassanizadeh, 2000), it was found that if values of μ_s were higher than that of μ_l, this was usually only by a factor of 2–3 and, occasionally, 6–8. Fig. 4 shows the corresponding residual values, i.e. the differences between observed and fitted concentrations on log scale. Because the tail of curve A deviates from the measured tail, residual values of the tail part become increasingly positive.

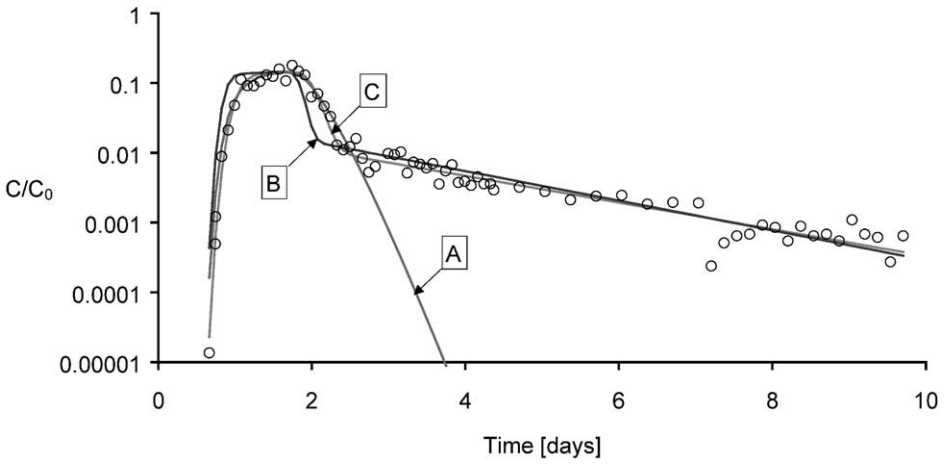

Fig. 3. Measured breakthrough curve (open circles) of MS2 in column I fitted with a one-site kinetic model (curves A and B) and a two-site kinetic model (curve C).

Table 2
Parameter values (in day $^{-1}$) estimated from breakthrough of MS2 in column III; A, B, and C in column headings correspond to curves A, B, and C in Fig. 3

Rate coefficients	A: One-site model	B: One-site model	C: Two-site model
k_{att1}	4.5	2.2	2.1
k_{det1}	5.0	0.074	0.054
k_{att2}			8.8
k_{det2}			42
$\mu_{s1} = \mu_{s2}$	3.9	0.48	0.43

In another set of simulations, again a one-site model was used, but this time, we used our model, EQ2KIN, with log-transformed concentrations and setting the parameter values for site 2 to zero. The corresponding parameter values are given under heading B of Table 2 and the corresponding curve B is also shown in Fig. 3. Note that this particular curve was forced to fit the maximum breakthrough concentration by giving this concentration extra weight; otherwise, the maximum breakthrough concentration would have been underestimated by about $0.5\log_{10}$. This time a perfect fit of the tail is obtained but the same discrepancies that were observed around the rising and declining limbs of breakthrough curves from the field study are seen here. These discrepancies are reflected in the residual values in Fig. 4 that are negative at the rising limb and positive at the declining limb of the breakthrough curve. The value of k_{det1} is now much less than that of k_{att1}.

Finally, the breakthrough curve was fitted by applying the two-site kinetic model. The estimated values are given under heading C of Table 2. The resulting curve C, in Fig. 3, clearly gives a very satisfactory fit to the measurements. This is also reflected by the corresponding residual values in Fig. 4, which are randomly scattered around zero, with an average residual of -0.0036 and a variance as small as 0.12. This implies that the assumption of log-normally distributed concentrations is reasonable. The height of the breakthrough curve is mainly determined by the values of k_{att1}, k_{att2}, k_{det2} and μ_l. The skewness of the rising and declining limbs is strongly affected by the value of k_{det2}. After

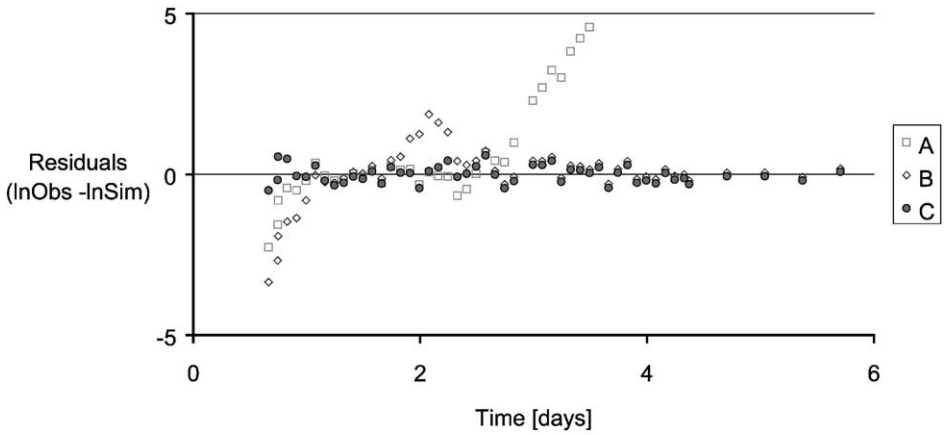

Fig. 4. Residual values (observed minus fitted values) on log-scale corresponding to models A, B and C in Fig. 3.

the pulse of viruses has passed, site 2 looses its influence on the shape of the curve because of the high detachment rate of this site. The tail of the breakthrough curve is mainly determined by the values of k_{det1} and μ_{s1}. Because the detachment rate from site 2 is relatively fast, there is little effect of inactivation of viruses that are attached to site 2. Consequently, estimates of μ_{s2} may not be meaningful. It was believed to be a reasonable assumption to set μ_{s2} equal to μ_{s1}; this was done in all of our simulations.

Figs. 3, 5a and 5b give the fitted breakthrough curves of MS2, PRD1 and ϕX174, respectively, in column I. Corresponding parameter values are given in Table 3. Parameters of the one-site model for MS2 and PRD1 have similar values. In the case of PRD1, the tail of the breakthrough curve appears to be curved and becomes flatter at the end. The one-site model does not follow this trend, whereas the two-site model does fit the slight bend of the tail. Compared to MS2, the values of k_{att2} and k_{det2} for PRD1 are smaller. The estimate of μ_s for PRD1 is now much smaller compared to the one-site model; it is only 50% greater than the μ_l value for PRD1. This is in agreement with the literature where the value of μ_s is found to be equal or slightly higher than that of μ_l (Blanc and Nasser, 1996; Schijven and Hassanizadeh, 2000). However, the value of μ_s for MS2 is found to be about five times higher than the value of its μ_l. This is probably overestimated. Also, the values of k_{att2} and k_{det2} are quite high and are most probably overestimated.

The breakthrough curve of ϕX174 is very much skewed to the right (Fig. 5b). The one-site model fits this curve badly, but the two-site model fits it very well. The goodness-of-fit (r^2) of the two-site model for ϕX174 was a bit lower than for MS2 and PRD1. Probably, the reason is that the counts of ϕX174 in the samples from the tail of the breakthrough curve were relatively low, resulting in a large variation in the observed concentrations. Consequently, it was difficult to get a reliable fit of the tail. Bacteriophage ϕX174 is relatively stable. Therefore, it was assumed that the inactivation coefficient of attached ϕX174 has the same value as that of free ϕX174. The curvature of its breakthrough tail is similar to that of PRD1, which is followed well by the two-site model.

All three bacteriophages attach relatively fast to site 1 and detach very slowly from this site, whereas both attachment to and detachment from site 2 are fast. Consequently, the removal rate coefficient λ is mainly determined by interaction with site 1, and only for a minor part by interaction with site 2.

The fact that the two-site model gives a better visual fit of the breakthrough curves is supported by the higher goodness-of-fit values for the two-site model than for the one-site model, although in the case of PRD1 this difference is small.

So far, estimates of model parameters had been obtained by fitting the observed breakthrough concentrations. This way, it appeared that a two-site kinetic model gives a better description of the breakthrough curves than a one-site kinetic model. In order to evaluate the two-site model further, parameter values obtained from column I breakthrough curves were used to predict the breakthrough curves from column II. The flow velocity in this column was 2.2 times higher than in column I. According to the colloid filtration theory (Yao et al., 1971), k_{att1} is proportional to $v^{1/3}$. Therefore, k_{att1} was increased by a factor 1.3. So, values of k_{det1}, k_{att2}, k_{det2}, μ_l, μ_{s1} and μ_{s2} were kept constant, but the value of k_{att1} was adjusted by a factor of 1.3. This simulation was carried out applying both the one- and two-site kinetic models. Figs. 5c, 5d and 5e show the predicted breakthrough curves.

In the case of MS2, both one- and two-site kinetic models slightly under-predict the maximum breakthrough concentration, and also the tail is lower. Both model predictions are in fact very similar. This is probably due to the fact that the tail of the breakthrough curve of MS2 in column I was straight. The prediction of the PRD1 breakthrough by the two-site model is very good, except for the discrepancy at the very end of the tail. The one-site model prediction and shows discrepancies at the beginning and the end of the tail of the breakthrough curve. In the case of ϕX174, the maximum breakthrough concentration is

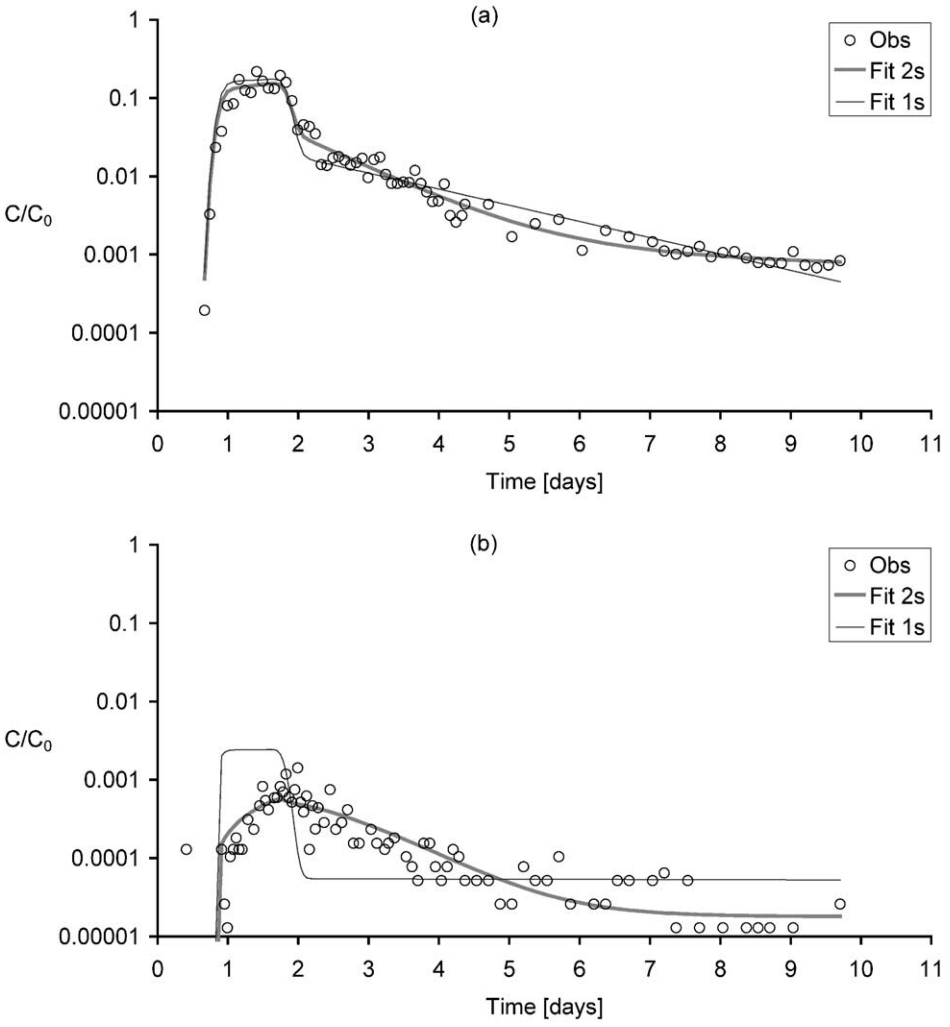

Fig. 5. (a)–(e) Breakthrough curves of bacteriophages. Circles are observations. The solid lines are the one- and two-site kinetic model fit. The dotted lines are the one- and two-site model predictions. In column II two times higher pore water velocity than in column I. (a) PRD1 in column I. (b) ϕX174 in column I. (c) MS2 in column II. (d) PRD1 in column II. (e) ϕX174 in column II.

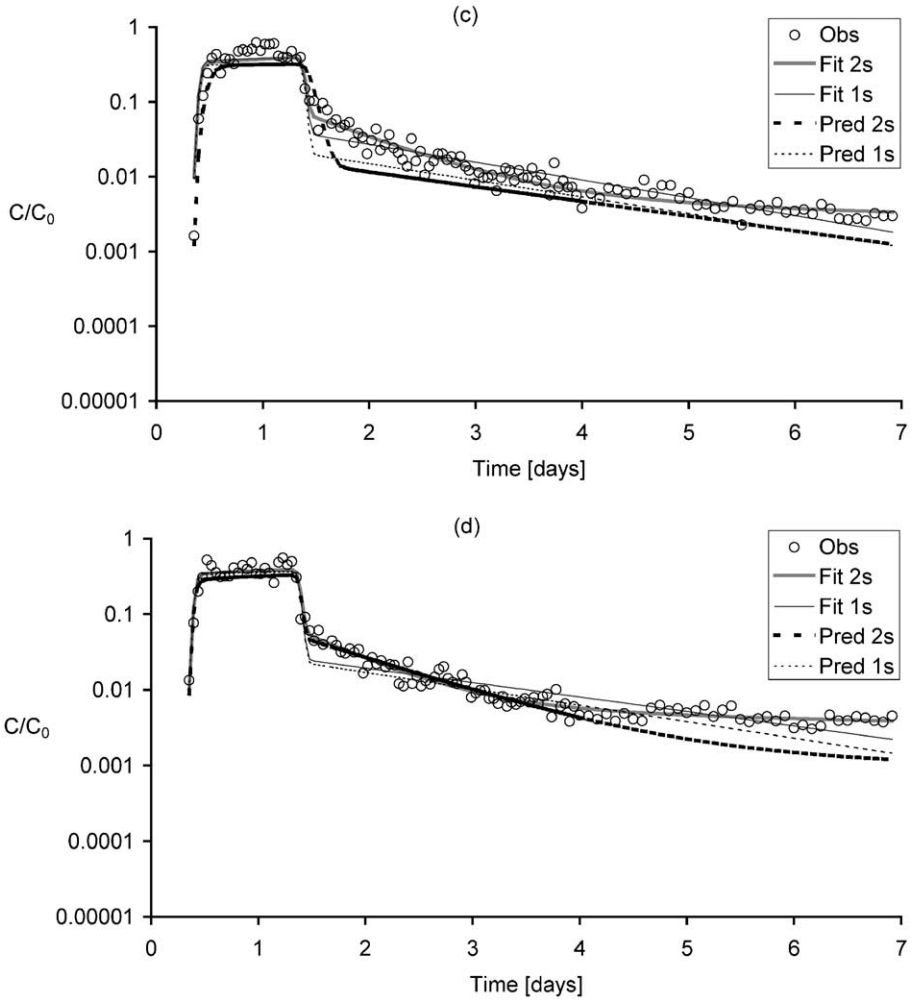

Fig. 5 (*continued*).

under-predicted by the two-site kinetic model, but it roughly follows the curvature of the tail. The prediction by the one-site kinetic model shows large discrepancies at the rising limb and at the beginning of the tail of the breakthrough curve.

Overall, predictions by the two-site kinetic model were reasonably good considering the goodness-of-fits between the predicted and observed concentrations, i.e. 84% (MS2), 89% (PRD1) and 75% (ϕX174). However, the same may be said for the predictions by the one-site model for MS2 and PRD1 with goodness-of-fits of 86% and 93%, respectively. The goodness-of-fit for the prediction of the ϕX174 breakthrough curve with one-site kinetic was much lower, 34%. This is mainly due to the strong skewness of the rising and declining limbs of the ϕX174 breakthrough curve.

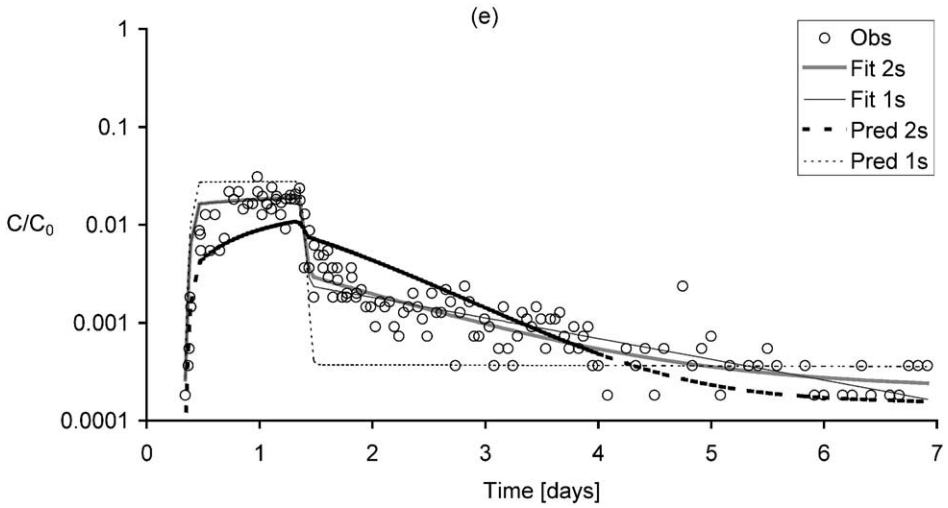

Fig. 5 (*continued*).

As an additional exercise, we fitted breakthrough curves of column II in order to obtain best-fit values of parameters of both models. Also, the 95% confidence intervals were determined. Results are given in Table 3. The fitted breakthrough curves are shown in Figs. 5c, 5d and 5e. Note that the dispersivities from columns I and II differed by almost a factor two (Table 1). This difference is probably due to some difference in packing of the columns. Nevertheless, these dispersivities are so low that they had little effect on fitting and simulation results. By applying dispersivity ranging from 4 to 16 mm, it was found that the fitted values of adsorption parameters did not change more than 5%.

We have found that in the case of MS2 and PRD1, for both one-site and two-site models, the predicted values of k_{att1} for column II (1.3 times the value of k_{att1} from the experiment with column I) fall within the 95% confidence interval of the best estimates of k_{att1}. In the case of ϕX174, the predicted values of k_{att1} fall just outside this 95% confidence interval. This suggests that our observations are consistent with the colloid filtration theory, which prescribes an increase in k_{att1} with a factor of $2^{1/3}$, i.e. 1.3 as a result at twice the velocity. This is also reflected in the best-fit values of the collision efficiency of site 1, α_1, which are more or less the same for both columns, for a given bacteriophage (compare values of α_1 for each bacteriophage under two-site model in Table 3).

Another interesting observation is that the values of k_{att2}, k_{det2} and μ_s for MS2 are now much smaller (compared to the values obtained from column I) and seem to be more realistic. The values of μ_s are almost the same as μ_l, just as what one would expect (Blanc and Nasser, 1996; Schijven and Hassanizadeh, 2000). As can be seen in Fig. 5c, the tail of

Notes to Table 3:
Dimension of parameters is day^{-1}. The values of μ_{s1} and μ_{s2} for ϕX174 were set equal to that of μ_l.
The estimated μ_l values were 0.082 day^{-1} (MS2), 0.044 day^{-1} (PRD1) and 0.012 day^{-1} (ϕX174).
The 95% confidence intervals are given between brackets.

Table 3
Parameter values from fitting breakthrough curves of bacteriophages in columns I and II

Bacteriophage	Column I			Column II		
	MS2	PRD1	ϕX174	MS2	PRD1	ϕX174
One-site model						
k_{att1}	2.2 (2.1–2.4)	2.0 (1.97–2.12)	7.0 (6.3–7.8)	2.5 (1.8–3.4)	2.5 (2.2–2.8)	10 (9.7–10.5)
k_{det1}	0.074 (0.050–0.11)	0.085 (0.075–0.096)	0.0039 (0.0031–0.0050)	0.14 (0.098–0.020)	0.089 (0.081–0.098)	0.046 (0.040–0.053)
μ_{s1}	0.48 (0.40–0.58)	0.47 (0.36–0.60)	0.012	0.48 (0.37–0.61)	0.40 (0.33–0.47)	0.53 (0.31–0.89)
α_1	0.0010	0.0012	0.0023	0.00061	0.0011	0.0023
r^2	80%	95%	–	96%	95%	90%
λ	2.0	1.8	5.3	2.0	2.1	9.3
% μ_l	4.1%	2.5%	0.2%	4.2%	2.1%	0.1%
% s1	95.9%	97.5%	99.8%	95.8%	97.9%	99.9%
k_{att1}/λ	1.1	1.2	1.4	1.2	1.2	1.1
$-\log_{10}(C/C_0)/x$	0.55	0.48	1.4	0.25	0.26	1.2
$-\log_{10}(C/C_0)/t$	0.86	0.76	2.2	0.86	0.91	4.0
Two-site model						
k_{att1}	2.1 (1.8–2.4)	1.9 (1.83–1.94)	8.0 (7.0–9.2)	2.1 (1.4–2.9)	2.2 (2.0–2.3)	9.5 (9.3–9.8)
k_{det1}	0.054 (0.045–0.065)	0.0045 (0.0036–0.0055)	0.0028 (0.0018–0.0045)	0.016 (0.011–0.023)	0.017 (0.016–0.018)	0.0031 (0.0026–0.0037)
k_{att2}	8.8 (6.5–12)	0.47 (0.41–0.53)	2.2 (1.4–3.7)	0.63 (0.58–0.70)	0.48 (0.44–0.53)	0.72 (0.63–0.83)
k_{det2}	42 (29–61)	1.1 (0.97–1.3)	1.2 (2.3–4.1)	1.4 (1.3–1.5)	1.6 (1.5–1.8)	0.96 (0.85–1.1)
$\mu_{s1} = \mu_{s2}$	0.43 (0.39–0.47)	0.064 (0.044–0.092)	0.012	0.075 (0.060–0.094)	0.065 (0.058–0.072)	0.012
α_1	0.00068	0.0011	0.0024	0.00051	0.00097	0.0022
α_2	0.0028	0.00027	0.00086	0.00016	0.00021	0.00016
r^2	96%	98%	83%	97%	98%	91%
λ	2.0	1.8	6.5	1.8	1.8	7.6
% μ_l	4.0%	2.4%	0.2%	4.5%	2.4%	0.2%
% s1	91.5%	96.2%	99.6%	93.6%	96.5%	99.7%
% s2	4.4%	1.4%	0.2%	1.9%	1.0%	0.1%
k_{att1}/λ	1.0	1.0	1.2	1.1	1.2	1.2
$-\log_{10}(C/C_0)/x$	0.56	0.50	1.8	0.23	0.22	0.95
$-\log_{10}(C/C_0)/t$	0.87	0.79	2.8	0.78	0.77	3.3

MS2 appears to flatten at the end (this was not the case in column I) and this is probably the reason that a lower value of μ_s is obtained.

Again, we see a much better visual fit of the breakthrough curves, especially of the curved tails, by the two-site model as compared to the one-site model. Nevertheless, the goodness-of-fit values found from fitting with the two-site model are only a few percent higher than with the one-site model.

Column experiments were carried out at low temperature (5 ± 3 °C), at which inactivation rates are low. As can be seen in Table 3 (see rows starting with λ and under), interaction with site 1 accounts for 92–97% of removal of MS2 and PRD1 and for almost 100% for removal of ϕX174. Because $k_{att1} \gg k_{det1}$, it follows from Eq. (9) that $\lambda \approx k_{att1}$, meaning that k_{att1} is the most important parameter for the removal of viruses at low temperatures. In other words, if one were interested in overall removal of viruses, a one-site kinetic model would be adequate for all practical purposes. Predicted removal with travel distance ($-\log_{10}(C/C_0)/x$) at twice the pore water velocity in column II is about half that in column I. Removal with travel time ($-\log_{10}(C/C_0)/t$) is hardly affected by pore water velocity, as one would expect.

5. Discussion and conclusions

The laboratory experiments reported here serve to gain insight in the kinetic modeling of breakthrough curves of viruses. One-site and two-site kinetic models have been employed. Breakthrough curves could be fitted and predicted satisfactorily by a two-site kinetic model, but not by a one-site kinetic model. Breakthrough curves that appear to be very skewed to the right, like that of ϕX174, are fitted poorly by a one-site kinetic model but a good fit is obtained using a two-site kinetic model. We contend that similarly shaped breakthrough curves reported for bacteriophages (Bales et al., 1991, 1993; DeBorde et al., 1998, 1999; Dowd et al., 1998), bacteria (Hornberger et al., 1992; Johnson et al., 1995; Lindqvist et al., 1994; McCaulou et al., 1994; Tan et al., 1994), *Cryptosporidium* (Harter et al., 2000) and colloidal particles (van de Weerd et al., 1998) can be satisfactorily simulated using a two-site kinetic model.

Tails of breakthrough curves that are measured long enough are not straight on a semi-log scale but curve up. Such tails cannot be simulated by a one-site model. In MS2 breakthrough curve of column I, this flattening of the tail of the breakthrough curve was not clearly observed, leading to about five times higher estimates of μ_s. Apparently, it is important to continue measurement of the breakthrough tails long enough to get a good estimate of μ_s. In column II, more pore volumes passed the column (about 14 pore volumes in 7 days) than in column I (about 10 pore volumes in 10 days). Thus, tails that are measured too short may lead to an overestimation of μ_s. This also leads to an overestimation of the values of k_{att2} and k_{det2}. It must be emphasized that an overestimation of μ_s always occurs if a one-site kinetic model is applied.

Although the two-site model fits the breakthrough curves better than the one-site model, leading to more accurate estimation of values of adsorption and inactivation parameters, we have found that overall removal rates predicted by either model are very

similar. That is to say, interaction with kinetic site 2, under the assumption that μ_{s2} equals μ_{s1}, only has a minor contribution to overall removal. Generally, $k_{att1} \gg k_{det1}$, $k_{att2} \leq k_{det2}$ and $k_{att2} < k_{att1}$.

The value of k_{att1} for ϕX174 were found to be higher than those for MS2 and PRD1. A similar difference in values of adsorption coefficients was also found between MS2 and ϕX174 in Ottawa sand at pH 7.5 by Jin et al. (1997, 2000). This is mainly due to the fact at pH 7.5–8.0, the dune sand is predominantly negatively charged and conditions are unfavorable for attachment to negatively charged viruses. Under such unfavorable conditions for attachment, the virus–grain interaction is the rate-limiting step for attachment and not the transport to the site by diffusion (Ryan and Elimelech, 1996). MS2 and PRD1 experience a greater electrostatic repulsion than the less negatively charged ϕX174, and thus adsorb less to site 1.

With some exceptions, values of k_{att2} and k_{det2} for all bacteriophages were of the same order of magnitude, despite the differences that exist in hydrophobicity and surface charge between the bacteriophages. This suggests that the nature of their interaction with sites of type 2 is neither electrostatic nor hydrophobic. Based on the shape of the salt breakthrough curves, we may exclude the so-called physical non-equilibrium effects, like distribution between mobile and immobile regions of water. The actual nature of the adsorption site 2 remains yet to be determined.

Another issue that could have affected our results is the aggregation of viruses. Although, this cannot be excluded with certainty, we believe it is most unlikely to have occurred in our case. Aggregation of phages has been discussed by Grant (1994), who applies a worst case where every collision of a phage particle with another phage particle would result in aggregation, which is unlikely considering their opposite charges. Only in lab stocks of 10^{12} pfu/ml, significant aggregation may occur. At 10^5 pfu/ml, used in our experiments, it is not expected to happen. Even if aggregates have formed in the cultured stock, they are most probably dispersed in the course of washing (with chloroform) and dilution. Moreover, the linearity of phage removal as a function of travel distance within a column, as well as the observed first order course of inactivation (Schijven, 2001), suggest that the existence of aggregates of phages is insignificant. Another strong indication is that no differences were seen using freshly prepared or 2-year-old phage suspensions (Schijven, 2001). In any case, the existence of phage aggregates cannot explain the curvature of the tail of the breakthrough curve.

Acknowledgements

This work was funded by the Ministry of Housing, Physical Planning and the Environment under project 289202, Water Microbiology.

W. Hoogenboezem and J. Bergsma (PWN Water Supply North Holland, The Netherlands) are greatly acknowledged for their support in obtaining sand samples, soil and water analyses. L.C. Rietveld and M. v.d. Meulen (Delft University of Technology) are thanked for the design and construction of the Perspex column supports.

References

Bales, R.C., Hinkle, S.R., Kroeger, T.W., Stocking, K., 1991. Bacteriophage adsorption during transport through porous media: chemical perturbations and reversibility. Environ. Sci. Technol. 25, 2088–2095.

Bales, R.C., Li, S., Maguire, K.M., Yahya, M.T., Gerba, C.P., 1993. MS-2 and poliovirus transport in porous media: hydrophobic effects and chemical perturbation. Water Resour. Res. 29, 957–963.

Bales, R.C., Li, S., Yeh, T.C., Lenczewski, M.E., Gerba, C.P., 1997. Bacteriophage and microsphere transport in saturated porous media: Forced-gradient experiments at Borden, Ontario. Water Resour. Res. 33, 639–648.

Blanc, R., Nasser, A., 1996. Effect of effluent quality and temperature on the persistence of viruses in soil. Water Sci. Technol. 33, 237–242.

Caldentey, J., Bamford, J.K.H., Bamford, D.H., 1990. Structure and assembly of bacteriophage PRD1, an *Escherichia coli* virus with a membrane. J. Struct. Biol. 104, 44–51.

Chu, Y., Jin, Y., 2001. Mechanisms of virus removal during transport in unsaturated porous media. Water Resour. Res. 37, 253–263.

DeBorde, D.C., Woessner, W.W., Lauerman, B., Ball, P.N., 1998. Virus occurrence in a school septic system and unconfined aquifer. Ground Water 36, 825–834.

DeBorde, D.C., Woessner, W.W., Kiley, Q.T., Ball, P.N., 1999. Rapid transport of viruses in a floodplain aquifer. Water Res. 33, 2229–2238.

Dowd, S.E., Pillai, S.D., Wang, S., Corapcioglu, M.Y., 1998. Delineating the specific influence of virus isoelectric point and size on virus adsorption and transport through sandy soils. Appl. Environ. Microbiol. 64, 405–410.

Fujito, B.T., Lytle, C.D., 1996. Elution of viruses by ionic and nonionic surfactants. Appl. Environ. Microbiol. 62, 3470–3473.

Grant, S.B., 1994. Virus coagulation in aqueous environments. Environ. Sci. Technol. 28, 928–933.

Harter, T., Wagner, S., Atwill, E.R., 2000. Colloid transport and filtration of *Cryptosporidium parvum* in sandy soils and aquifer sediments. Environ. Sci. Technol. 1, 62–70.

Havelaar, A.H., Hogeboom, W.M., Pot, R., 1984. F-specific RNA-bacteriophages in sewage: methodology and occurrence. Water Sci. Technol. 17, 645–655.

Hornberger, G.M., Mills, A.L., Herman, J.S., 1992. Bacterial transport in porous media: evaluation of a model using laboratory observations. Water Resour. Res. 28, 915–938.

ISO (International Organization for Standardization), 2000a. Water quality—Detection and enumeration of bacteriophages—Part 1: Enumeration of F-specific RNA-bacteriophages. ISO 10705-1, Geneva.

ISO (International Organization for Standardization), 2000b. Water quality—Detection and enumeration of bacteriophages—Part 2: Enumeration of somatic coliphages. ISO 10705-2, Geneva.

Jin, Y., Yates, M.V., Thompson, S.S., Jury, W.A., 1997. Sorption of viruses during flow through saturated sand columns. Environ. Sci. Technol. 31, 548–555.

Jin, Y., Chu, Y., Li, Y., 2000. Virus removal and transport in saturated and unsaturated sand columns. J. Contam. Hydrol. 43, 111–128.

Johnson, W.P., Blue, K.A., Logan, B.E., Arnold, R.G., 1995. Modeling bacterial detachment during transport though porous media as a residence-time dependent process. Water Resour. Res. 31, 2649–2658.

Kinoshita, T., Bales, R.C., Maguire, K.M., Gerba, C.P., 1993. Effect of pH on bacteriophage transport through sandy soils. J. Contam. Hydrol. 14, 55–70.

Lindqvist, R., Cho, J.S., Enfield, C.G., 1994. A kinetic model for cell density dependent bacterial transport in porous media. Water Resour. Res. 12, 3291–3299.

Loveland, J.P., Ryan, J.N., Amy, G.L., Harvey, R.W., 1996. The reversibility of virus attachment to mineral surfaces. Colloids Surf., A 107, 205–221.

Lytle, C.D., Routson, L.B., 1995. Minimised virus binding for test barrier materials. Appl. Environ. Microbiol. 61, 643–649.

McCaulou, D.R., Bales, R.C., McCarthy, J.F., 1994. Use of short-pule experiments to study bacteria transport through porous media. J. Contam. Hydrol. 15, 1–14.

Penrod, S.L., Olson, T.M., Grant, S.B., 1996. Deposition kinetics of two viruses in packed beds of quartz granular media. Langmuir 12, 5576–5587.

Ryan, J.N., Elimelech, M., 1996. Colloid mobilization and transport in groundwater. Colloids Surf., A 107, 1–56.

Schijven, J.F., 2001. Virus Removal from Groundwater by Soil Passage: Modeling, Field and Laboratory Experiments. PhD thesis, Delft University of Technology, ISBN 90-646-4046-7.

Schijven, J.F., Hassanizadeh, S.M., 2000. Removal of viruses by soil passage: overview of modeling, processes and parameters. Crit. Rev. Environ. Sci. Technol. 30, 49–127.

Schijven, J.F., Hoogenboezem, W., Hassanizadeh, S.M., Peters, J.H., 1999. Modeling removal of bacteriophages MS2 and PRD1 by dune recharge at Castricum, The Netherlands. Water Resour. Res. 35, 1101–1111.

Shields, P.A., Farrah, S.R., 1987. Determination of the electrostatic and hydrophobic character of enteroviruses and bacteriophages, abstr, Q-82. Program Abstr. 87th Ann. Meet. Am. Soc. Microbiol. American Society for Microbiology, Washington, DC.

Tan, Y., Gannon, J.T., Baveye, P., Alexander, M., 1994. Transport of bacteria in aquifer sand: experiments and model simulations. Water Resour. Res. 12, 323–3252.

Toride, N., Leij, F.J., van Genuchten, M.T., 1995. The CXTFIT code for estimating transport parameters from laboratory or field tracer experiments, Version 2.0 US Salinity Laboratory. Agricultural Research Service. US Department of Agriculture, Riverside, CA, Report No. 137.

van de Weerd, H., Leijnse, A., van Riemsdijk, W.H., 1998. Transport of reactive colloids and contaminants in groundwater: effect of nonlinear kinetic interactions. J. Contam. Hydrol. 32, 313–331.

Yao, K.M., Habibian, M.T., O'Melia, C.R., 1971. Water and waste water filtration: concepts and applications. Environ. Sci. Technol. 5, 1105–1112.